Diffuse Back-Illuminated Extinction Imaging of Soot: Effects of Beam Steering and Flame Luminosity

Karl Oskar Pires Bjørgen, David Robert Emberson, Terese Løvås
Department of Energy and Process Engineering, Norwegian University of Science and Technology, Trondheim, Norway

Abstract

This study presents diagnostic development of diffuse back-illuminated extinction imaging of soot. The method provides high temporal and spatial resolution of the line-of-sight optical density of soot (*KL*) in compression-ignited fuel sprays relevant to automotive applications. The method is subjected to two major sources of error, beam steering effects and broadband flame luminosity effects. These were investigated in detail in a direct injection combustion chamber with diesel fuel, under high and low sooting conditions. A new method for correcting flame luminosity effects is presented and involves measuring the flame luminosity using a separate high-speed camera via a beam splitter. The new method and existing methods are applied and the resulting flame luminosity correction errors are compared. The new method yields 50% lower errors than the most promising method (optical flow method). The impact on *KL* was investigated, showing that the *KL* uncertainty when using the optical flow method is unbounded for *KL* values above 2.7, while the new method has an uncertainty of 0.5 for the maximum *KL* value of 3.8. The new method yields overall lower uncertainties and is more suited to measuring *KL* in optical thick conditions. Large refractive index gradients in the path of the incident light cause false attenuation, resulting in ambiguity of the measured *KL*, referred to as beam steering. A detailed investigation of the beam steering effects caused by the non-uniformities in the diffused light source was performed. A beam steering model was made and qualitatively validated from experiments. The results from the beam steering model showed the importance of having a large collection angle, in order to average out small-scale non-uniformities in the light source. The model also showed that large-scale non-uniformities in the light source could affect the measurement even if the collection angle is large.

Introduction

The understanding of in-flame combustion processes resulting in soot formation and oxidation is of great importance since the underlying physical phenomena are not fully understood, especially for oxygenated fuels such as biofuels. Numerical simulations provide insight to complex processes that are hard to capture in physical experiments, but the models used for running the simulations require validation from experimental results. Temporally and spatially resolved in-flame soot measurements in engines are hard to perform since the process occurs over a few milliseconds, optical access is usually limited, and the environment in the combustion chamber is harsh, i.e. large density gradients, high temperature and high concentrations of soot. The in-flame measurements are thus prone to large errors.

Several methods for quantifying the concentration of in-flame soot exists and it is extensively reported in literature. A commonly used technique is the two-color method, where the incandescence of the soot particles are measured at two wavelengths. Based on the soot incandescence radiance measurement made at two different wavelengths and the semi-empirical soot emissivity model proposed by Hottel and Broughton [1], the optical depth (*KL*) can be calculated. However, the method introduces a large uncertainty on the *KL* [2].

Another well-established method for in-flame soot measurement is the planar laser-induced incandescence (PLII) [3]. The soot particles are heated up by a laser sheet to temperatures much higher than the surrounding gas temperature. The laser-induced incandescence is then measured by an intensified charge-coupled device (CCD) camera, providing a planar measurement of the soot distribution. Together with laser extinction, the soot concentration in the measured plane can be determined. In an engine application, the main limitation of PLII is the relatively low repetition rate of the laser and attenuation of the incandescence signal in the soot cloud [4].

A more reliable method for measuring the in-flame soot concentration is laser extinction [5]. The optical measurement is based on the scattering and absorption of the laser intensity by the soot particles. By measuring the ratio of the transmitted laser intensity and the original laser intensity, *KL* can be obtained. The measurement is a line-of-sight measurement through a point in the soot cloud.

The method presented in this study is diffuse back-illuminated extinction imaging (DBIEI) of soot particles. The method is based on the light extinction from particles present in the light path, where the extinction of light is the sum of the light intensity scattered and absorbed by the particles. Similar to the laser extinction method, DBIEI of soot is a line-of-sight measurement, but instead provides an instantaneous two-dimensional measurement of *KL*. The optical depth *KL* can be calculated from measuring the ratio between the transmitted light intensity I_t and the original light intensity I_o, described by the well-known Beer-Lambert law [6]:

$$\frac{I_t}{I_0} = e^{-KL} \tag{1}$$

KL is the product of the dimensional extinction coefficient *K* and the path length *L* through the particle cloud. By knowing the local path length *L*, *K* can be calculated locally. The soot volume fraction f_v can further be calculated from small particle Mie theory [6]:

$$f_v = \frac{K\lambda}{k_e} \quad (2)$$

where λ is the wavelength of the incident light and k_e is the dimensionless extinction coefficient. k_e can be determined from knowing the in-flame optical and physical properties of soot [7]. However, this imposes large uncertainties on the measurement since the optical and physical properties of soot are constantly varying throughout the combustion process. To determine f_v from *KL* requires detailed knowledge of the in-flame soot aggregate structure, for instance measured from transmission electron microscope images, and the local path length *L*. Since this study is focused on the DBIEI of soot technique, only *KL* is considered.

There has been several proposed setups for extinction imaging of soot in the past: e.g., Greenberg and Ku [8], Xu and Lee [9], Thomson et al. [10], Ghandi and Heim [11] and Westlye et al. [12]. Only Westlye et al.'s setup has been designed specifically for the harsh conditions present in compression ignition (CI) engines. The optical dimensioning described is focused on abatement of beam steering effects on *KL*. Beam steering of the incident light happens due to changes in refractive index of the gas in the combustion chamber. These refractive index changes arise due to the large density gradients present in the combustion chamber, resulting from the pressure and temperature variations during combustion. The incident light traverses this region with large changes in refractive index, which causes the light to diverge from its original path (the light beam is steered). If the divergence of the light ray is large enough, it is steered in or out of the light collection system, causing a false extinction of the back-light. The effect is similar to what can be observed in the schlieren technique for detection of gas density gradients. The beam steering effects should be abated as much as possible in a soot measurement system, as the attenuation of the light due to beam steering cannot be distinguished from the attenuation due to soot. These effects are severe in a typical CI fuel spray and must be assessed when setting up a DBIEI of soot measurement system.

The DBIEI setup described by Westlye et al. [12] is an evolution of the Ghandi and Heim setup [11]. The setup consists of a high-intensity pulsed light emitting diode (LED) placed in front of a Fresnel lens which collimates the light and directs it onto a large engineered diffuser. The engineered diffuser diffuses the light within a predefined angle, and ensures the light source to be near-Lambertian and extended. The diffused light is then directed through the combustion chamber. Based on theoretical descriptions, the work concludes that the diffused light source should be extended and spatially uniform with a constant radiance. Furthermore, measurement techniques are suggested for characterizing the optical setup and the diffused light source. Also geometrical constraints are described in order to ensure beam steering abatement.

Musculus and Pickett [13] addresses the issue of beam steering of a laser beam traversing a combustion chamber. The laser beam is steered away from its original path by the large density gradients in the combustion gases and poses a concern in that signal is lost if the beam is steered outside the collection aperture. In order to avoid the loss of signal, a large aperture and an integrating sphere was used on the collection side such that the beam intensity could be measured without being affected by beam steering. Furthermore, they also measured the divergence angle of the beam steering during CI engine conditions in an optical engine by varying the aperture size of the collection system. Full-angle beam divergence of over 100 mrad was measured and 95% of the beam steering occurred within 50 mrad.

In addition to beam steering effects, flame luminosity effects must be considered when measuring *KL* in a DBIEI setup. A CI spray flame emits strong broadband radiation (flame luminosity) which is superimposed on top of the transmitted light signal used in the DBIEI system. Any system that is to accurately measure *KL* must keep any influence of the flame intensity signal to a minimum and/or post-process the flame intensity signal out. Descriptions of different methodologies for correction of the flame luminosity intensity are presented in [14].

Soot measurements using DBIEI has previously been applied by Pastor et al. in [15] and [16] for measuring *KL* in 30% Decane and 70% Hexadecane fuel sprays and sprays of Diesel/Gasoline blends, respectively. The evolution of the *KL* distributions were presented as ensemble averages of several injections. The flame luminosity correction method used was subtracting the ensemble average of the flame luminosity distribution from the ensemble averaged transmitted light measurement. Hence, these measurements did not provide instantaneous *KL* distributions, but instead an ensemble averaged *KL* evolution. The flame correction errors are not discussed in this study, while the uncertainty on *KL* from beam steering effects were estimated to be below 0.1.

Skeen and Yasutomi [17] used DBIEI of soot based on Westlye et al. [12] to quantify the temporal evolution of soot and total soot mass formed in a n-dodecane spray pyrolysis. The flame luminosity is measured and subtracted from the measurement by alternating the light source every second frame, but the estimation method used is not described in detail, nor is the uncertainty on *KL*.

Pandurangi et al. [18] presents a numerical model for simulating soot processes in a n-dodecane fuel spray (Engine Combustion Network (ECN) Spray A reference case [19]). The numerical results were validated with experimental measurements of *KL* using DBIEI based on Manin et al. [7] and Skeen et al.'s work [20]. Also here the flame luminosity was corrected for by alternating the light source. The subtraction of the flame luminosity from the transmitted image resulted in some negative values on the corrected transmitted image. This was minimized via a weighted temporal averaging scheme, i.e. not providing the instantaneous *KL* distribution. The estimated uncertainty on the temporally averaged *KL* for the higher temperature cases was ±10%.

In this study we present a novel methodology for flame luminosity correction in a high temporal DBIEI system, which we show that minimizes the uncertainties of the measured *KL*. The errors connected to the flame luminosity correction methods proposed in previous studies will be compared to the new method proposed in this work. In addition, beam steering effects due to non-uniformities of the light distribution from the engineered diffuser will be investigated, and its related errors quantified.

Materials and Methods

Optical Chamber

Chamber Design

All experiments were performed using the Optical Accessible Compression Ignited Chamber (OACIC) at the Department of Energy and Process Engineering at the Norwegian University of Science and Technology (NTNU). The OACIC is a reciprocating rapid compression machine equipped with windows, enabling line-of-sight optical measurements of the reacting spray under CI engine conditions. The OACIC is a redesigned cylinder head of a large bore, single cylinder 4-stroke CI engine (Lister 12 CS). The combustion chamber is cylindrical in shape, 50 mm in diameter and 40 mm deep, sealed with two fused-silica windows 25 mm thick, 63 mm in diameter. The engine's swept volume and the chamber are connected via a connecting throat, which is removable. This throat may be modified to introduce increasing amounts of swirl into the chamber. For this study, a throat with minimal swirl was used. Optical access is 50 mm in diameter and the windows are retained by conically shaped rings in order to maximize the angular access to the chamber. The chamber utilizes the original intake and exhaust valves and is equipped with a second generation, Bosch solenoid common rail injector. For all experiments reported in this study, the amount of fuel injected was small and the chamber was operated in a skip fire mode, hence no mechanical work is extracted from the OACIC. The engine's original crankcase and crankshaft is utilized and is connected to an AC dynamometer. The crankshaft position is tracked by a magnetic shaft encoder with 3200 readings per revolution, giving a resolution of ~0.11 crank angle degrees (CAD) to the injection location and chamber pressure measurement. The OACIC is installed with a dynamic pressure sensor (Kistler 6052C) to collect motored and combustion pressures. The inlet air is compressed by a roots compressor with the air pressure measured (absolute pressure, Kistler 6011) at the inlet manifold. The inlet air is also heated after the compressor by a 2 kW electric flow heater. This enables the inlet air to be heated to a maximum temperature of 150 C^{o} and compressed to 1.6 bar. The injector is connected to a common-rail fuel system and can be pressurized up to 1500 bar by an air-driven fuel pump. The nozzle used is a modified Bosch nozzle (DSLA124P1659) with a single hole of 0.12 mm in diameter. The data acquisition, temperature control, tracking of crank position and triggering of injector are all programmed in Labview. Geometrical information of the OACIC can be found in Table 1.

Table 1. Geometrical information of the OACIC.

Bore	130 mm
Stroke	140 mm
Compression ratio	15.93
Displaced volume	1.9 L

Operating Conditions

The target injection pressure was 1000 bar for all injections. The fuel used was a commercial Diesel fuel (EN590). The target condition in the OACIC at top dead center (TDC) was chosen to be 17.5 kg/m^3 gas density, 835 K ambient gas temperature for the low sooting case (LS), and 929 K for the high sooting case (HS). The resulting target pressure in the chamber at TDC was 42.1 bar for the LS condition and 48.8 bar for the HS condition. The conditions were chosen based on typical engine operating conditions. The start of energizing (SOE) of the injection occurred 2 CAD before top dead center (BTDC), and the injection duration was 4 ms. The crankshaft speed was 500 rpm, which ensures near-constant thermodynamic conditions during the combustion event. The operating conditions are summarized in Table 2.

Table 2. Operating conditions.

Density TDC	17.5 kg/m^3
Temperature TDC (LS/HS)	835 K/929 K
Pressure TDC (LS/HS)	42.1 bar/48.8 bar
O_2 concentration	21%
Injection pressure	1000 bar
Speed	500 rpm
Injection timing	2 CAD BTDC
Injection duration	4 ms

Optical Setup

The DBIEI setup for measuring soot used in this study is shown in Figure 1. The setup consists of a light source side and a collection side. The aim of the optical setup is to ensure that the light input to the engineered diffuser is collimated, uniformly distributed and covers a large enough area of the diffuser. These requirements must be upheld while maximizing the light throughput, since a higher light intensity reduces errors related to flame correction. The degree of collimation of the input light to the diffuser has a direct influence on the angular distribution of the output light from the diffuser, which can result in beam steering effects. This is addressed by dimensioning the setup according to requirements limited by the beam steering angle occurring in the chamber, as will be discussed later.

On the light source side, a square SST-90-R LED (centered at ~628 nm, FWHM 15 nm) from Luminus Devices Inc. was used. The LED was pulsed by an in-house built circuit based on the design of Willert et al. [21]. The circuit produces very short pulses (down to ~500 ns) with high currents at frequencies up to ~100 kHz. The pulsing of the LED allows the forward current of the LED to exceed its rated limit and consequently maximizing the radiant flux emitted, in comparison to continuous mode where the LED is damaged when exposed to the same current. The driver voltage was set to 36 V and the pulse duration was 1.33 µs. The LED was pulsed at 37.5 kHz, resulting in a duty cycle of 5% (1.33 µs pulses with 26.67 µs period). The LED light response was aligned with the camera exposure in such way that the camera was exposed to as much light as possible.

The LED has a glass dome over the emitting surface, which ensures the light to be Lambertian within approximately 40 degrees full angle. In front of the LED, two identical 25 mm diameter aspheric condenser lenses (Thorlabs, Inc. ACL25416U-A) oriented in opposite position to each other were used to gather and focus the light onto the collimating lens, minimizing waste of light from the LED to the collimating lens. The collimating lens was a 100 mm diameter lens with focal length of 100 mm and was placed 100 mm from the focal point of the aspheric condenser lenses, ensuring that the light from the LED was collimated. The engineered diffuser was placed 90 mm from the collimating lens (measured from the flat side of the collimating lens to the diffuser surface), while the diffuser was placed

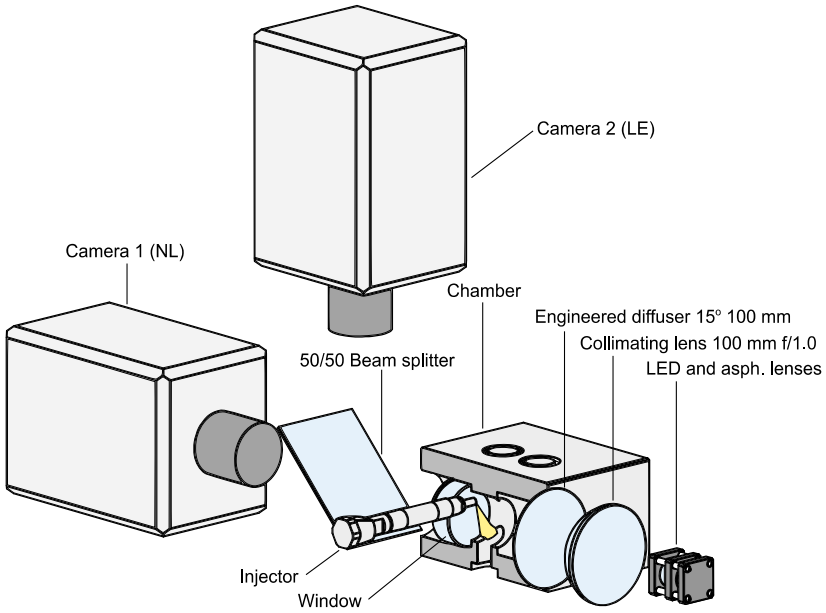

Figure 1. The optical setup for DBIEI of soot.

106 mm from the focal plane in the chamber. The 100 mm diameter engineered diffuser had a divergence angle of 15 degrees full angle (RPC Photonics, Inc. EDC-15-15132-A).

On the collection side, two high speed cameras (Photron, FASTCAM SA1.1 and SA5) were used for imaging the same field of view via a 50/50 beam splitter for visible light, details on the technique will follow later in this section. Both cameras were equipped with the same collection optics and spectral filter. The objective lens used was a 50 mm Nikkor f/1.2 with a 500D close-up lens in order to be able to focus close. The distance between the objective lens and the focal plane of camera 1 was 440 mm and 435 mm for camera 2. The resolution used was 320x192 for both cameras, resulting in a pixel size of 0.162 mm/pixel for camera 2. The bandpass filter used was a red filter centered at 634 nm (FWHM 70 nm). The bandpass filter suppresses most of the broadband radiation from the flame, but lets the light from the LED through. Due to wavelength emission shifting of the LED when driving at high currents, a relatively wide bandpass filter of FWHM 70 nm was chosen, since the exact wavelength band that the LED emits in is not accurately known. Using this bandpass filter ensured all LED light is transmitted to the camera sensor. The aim is to maximize the ratio of radiance received from the light source to radiance received from the flame radiation. This can be achieved by increasing the power of the light source and/or using a narrow bandpass filter centered on the peak wavelength of the light source. In addition, a combination of absorptive neutral density (ND) filters were used in front of the objective lens in order to adjust the amount of light exposed to the cameras, since the exposure time and the aperture size are fixed. In this way, the entire dynamic range of the camera is utilized. Camera 1, which only measures the natural flame luminosity (NL), was equipped with ND filters corresponding to 1.5 in optical density (OD), whilst camera 2, which measures both NL and the light extinction signal (LE), had filters corresponding to 1.8 OD. Since camera 1 only measures flame luminosity, the OD is lower in order to obtain more information on the flame luminosity intensity levels. For camera 2, the OD was chosen such that the back-light was close to the maximum intensity level of the camera (12-bit dynamic range, 4095 counts).

In previous setups [14], artifacts on the measurement due to internal reflections in the filter pack has been observed. This was checked for by inspecting the *KL* measurements for a high sooting flame in detail. No effects of this was observed in the current setup for several filter configurations. Reflections from the second surface of the beam splitter was also considered. However, according to the specification of the beam splitter, less than 2% is reflected off one of the surfaces due to the use of anti-reflective coating, resulting in a negligible effect on the measurement.

Optical Characterization

In order to abate beam steering effects, the optical setup needs to be properly characterized and dimensioned according to the beam steering that could be expected to occur in the OACIC during a CI spray combustion event. The geometrical description of the current optical setup is shown in Figure 2. The OACIC in the figure is shown as a cross-sectional cut in the center of the combustion volume, all dimensions are correctly scaled relative to each other. The vertical dotted line in the middle represents the focal plane of the objective lens, which was located 435 mm from the objective lens (camera 2). The rays crossing in the focal plane are enclosing the acceptance cone of a single pixel on the imaging sensor, showing where on the diffuser surface light is collected from, and at what angles the light is collected. The angles are dependent on the distance between the focal plane and the objective lens, and the aperture size. The acceptance cone angle is denoted as ω, the steepest angle found in the acceptance cone is α and the full diffusing angle is β. The steepest angle α is measured from the central axis to the steepest light ray within the acceptance cone. For the acceptance cone of the central pixel, $\alpha = \omega/2$.

Because the objective lens was focused closer than infinity, the acceptance angle ω could not be calculated from the focal length and the f-number. Consequently, the acceptance angle for the central pixel and a peripheral pixel was measured by the method described in [12]. The peripheral pixel was located ~20 mm from the central pixel in the focal plane. The acceptance angles for the peripheral and the central pixel were determined to be $\omega = 5.15^{\circ}$ and $\omega = 5.34^{\circ}$,

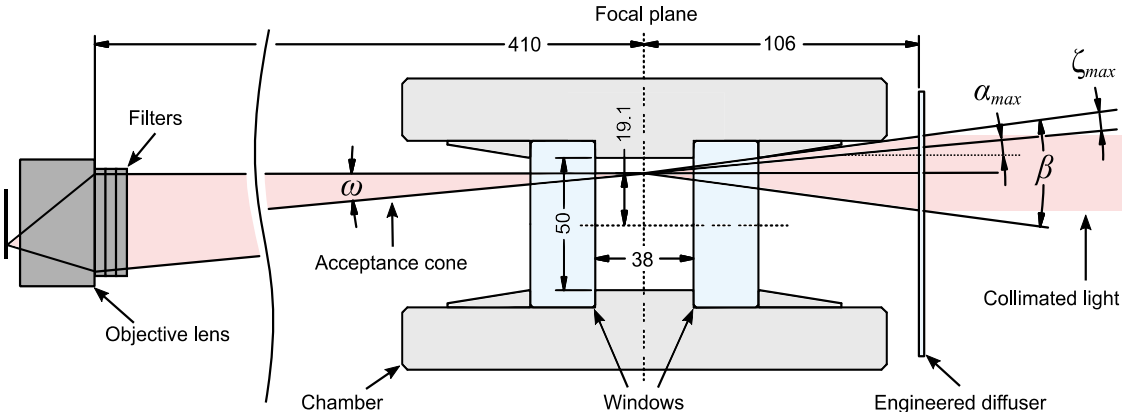

Figure 2. The geometrical dimensions of the optical setup. The acceptance cone for the most peripheral pixel is shown. ω = 5.15˚ is the acceptance angle and ζ_{max} = 2.36˚ is maximum beam steering angle abated by the system, β = 15˚ is the full diffusing angle and α_{max} = 5.14˚ is the steepest angle for the peripheral pixel.

respectively. Based on this, the steepest angle in the acceptance cone for the peripheral pixel (α_{max}) was found to be 5.14˚. The full angle beam steering 2ζ measured in [13] is 50 mrad (2ζ = 2.86˚ for 95% of the occurrence of beam steering) for a typical CI combustion. For the current setup, the acceptance cone is always within the angular domain of the diffused light, i.e. $\alpha < \beta/2$, meaning that the criterion needed to be fulfilled in order to avoid beam steering effects is

$$\beta > 2\alpha + 2\zeta \tag{3}$$

With the dimensions for the current setup, this criterion is fulfilled. According to the beam steering angle mentioned, the requirement for the divergence angle of the engineered diffuser is β > 13.1˚. With β = 15˚ and 2α_{max} = 10.28˚, the system can abate beam steering effects for ray deflections up to 2ζ_{max} = 4.72˚ (82 mrad full angle beam steering).

In addition to dimensioning the optical system properly for abating the beam steering effects, the angular distribution of the diffused light was also measured. The procedure for this can be found in [12]. The purpose of the measurement is to verify that the light source is Lambertian within the angular domain of the diffused light, i.e. the radiance received by a pixel is independent of the collection angle. The result of the measurement is shown in Figure 3 for a central and a peripheral position (20 mm from the center) in the focal plane. The result shows that within the 15 degree angle of the diffuser (7.5 degrees either side of 0 degrees), the light intensity at the focal plane is reasonably constant, hence the angular distribution of the setup was found to be satisfactory.

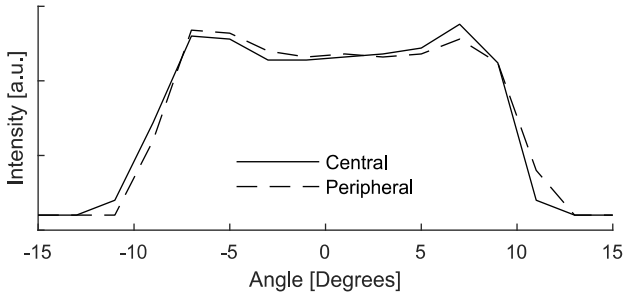

Figure 3. Angular intensity distribution of the engineered diffuser.

Flame Luminosity Correction Methods

The measured light intensity I_{tf} is the summation of the intensity of light transmitted through the sample region (I_t) and the flame luminosity (I_f). The intensities I are from here on referred to as images, i.e. two-dimensional arrays of light intensities measured simultaneously. In order to obtain the KL of the soot present in the chamber, the flame luminosity needs to be estimated or measured separately so that I_t can be determined. In previous studies using 2D light extinction for high temporal measurements, this has been achieved by alternating the light source with the camera exposures in order to capture an image containing I_f only, before and after the I_{tf} measurement. Westlye [14] investigated different approaches in order to predict I_f during the I_{tf} measurement (e.g., the mean image method and the optical flow method). The simplest approach is to take the pixel-wise mean of I_f before and after I_{tf}, i.e. the mean image method,

$$I_f = (I_{f-1} + I_{f+1})/2 \tag{4}$$

where I_{f-1} is the flame luminosity image before and I_{f+1} is the image after I_{tf}.

Optical Flow Method

An improved I_f estimation can be achieved by calculating the optical flow field based on the flame image before and after I_{tf}. The estimated optical flow field based on the image sequence is calculated from an algorithm given by Sun et al. [22]. The result from the algorithm is a vector field $U(x,y,t)$ describing the spatial movement of all pixel values from the one frame to another. Since $U(x,y,t)$ is calculated from I_{f-1} and I_{f+1}, half of the movement is used in order to estimate the movement from I_{f-1} to I_f, i.e.

$$\begin{aligned} U &= opticalflow(I_{f-1}, I_{f+1}) \\ I_f &= reconstruct(I_{f-1}, U/2) \end{aligned} \tag{5}$$

The estimated image I_f is reconstructed from I_{f-1} by translating the pixel values according to the optical flow field velocity vectors divided by two, i.e. half way. By applying this procedure both forward and backward, and averaging the result, a more precise estimation of I_f is achieved. This method becomes more accurate with smaller intensity translations between each frame, i.e. by increasing the frame rate, smaller errors to the estimation can be achieved.

Two-camera Method

The new method proposed in this study, for determining I_f, is by measuring it using a separate high speed camera. As seen in Figure 1, a 50/50 beam splitter for visible light was used on the collection side in order to image the flame from the same angle with two cameras. The camera exposures were synchronized and recording at 75 kfps. Camera 1 was only measuring the flame luminosity, which is denoted as I_f^*, whilst camera 2 was measuring the alternating frames of flame luminosity plus transmitted light (I_{tf}) and flame luminosity (I_f). This was achieved by adding a small delay of Δt = 1.64 µs to the exposure of camera 2 with respect to the exposure of camera 1, see Figure 4. The LED circuit was triggered by the camera 1 exposure, the position and width of the LED pulse was modified to fit the exposure of camera 2 via a signal generator. The exposure of the cameras were both set to 1 µs. A photodiode measuring the LED light pulse was used to ensure that no light from the LED was captured by the camera 1 exposure. Camera 1 therefore measured the flame luminosity distribution I_f^* 1.64 µs before camera 2. In this way, I_f^* was used to correct for the flame luminosity in I_{tf}.

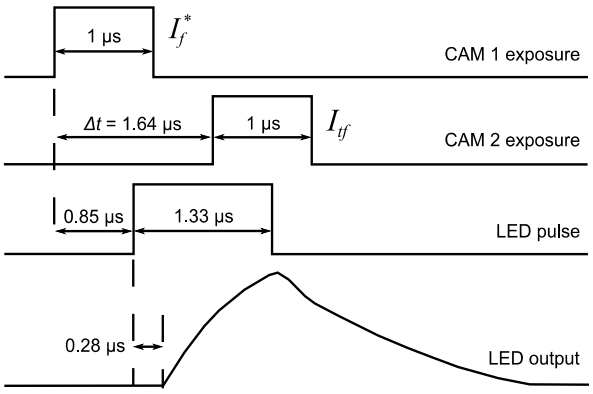

Figure 4. Timing of exposures, the LED trigger pulse and the LED output response.

When comparing I_f^* and the real I_f to each other before post-processing, differences between them occur due to misalignment between camera 1 and 2, and the intensity levels are not the same because two different imaging sensors are used. Correct alignment of the two cameras was found to have a large impact on the quality of the measurement. The largest alignment influence on the quality was on the rotational orientation of the cameras to the focal plane, i.e. the parallelism of the cameras sensors to the focal plane, whilst the measurement was relatively insensitive to any translational misalignment. This is due to the three-dimensional structure of the flame. A good rotational alignment was achieved by focusing the cameras to a point a short distance away, and then to a point further away, and checking that the points were located in the same location relative to each other on both cameras. This procedure resulted in a significant improvement on the measurements. It is essential that the same collection optics for each camera are used, which was the case here.

In Figure 5, the post-processing scheme is summarized. Samples of three images from both cameras are displayed, i.e. I^*_{f-1}, I_f^* and I^*_{f+1} for camera 1, and I_{f-1}, I_{tf} and I_{f+1} for camera 2. The flame luminosity images measured by camera 1 closely match the flame luminosity images measured by camera 2, due to the very short time step (Δt = 1.64 µs) between them. The aim of the measurement is to eliminate the flame luminosity (I_f) from the I_{tf} image, i.e. I_f is estimated based on I_f^* from camera 2. However, the flame images from camera 1 are slightly misaligned compared to camera 2, and the intensity levels do not match. Information on the misalignment and scaling is retrieved by comparing I^*_{f-1} and I_{f-1} through an optimization algorithm. The images are processed using a Matlab function called *imregtform*, which is an intensity-based image registration algorithm and outputs a geometric transformation matrix. The algorithm translates, rotates, scales and warps (shear) I^*_{f-1} until it matches I_{f-1} within a predefined threshold or after a number of iterations. The transformation matrix obtained is then applied to I_f^* in order to obtain I_f. In addition, the intensity level of I^*_{f-1} is optimized through two methods in order to match I_{f-1}. The first method is a simple pixel intensity scaling optimizer, where the scaling factor that results in least residuals on the absolute difference between I^*_{f-1} and I_{f-1} ($\Delta I_{f-1} = |I^*_{f-1} - I_{f-1}|$) is applied to I_f^*. The second approach used is histogram-matching (*imhistmatch* in Matlab). The algorithm compares the intensity histograms of I^*_{f-1} and I_{f-1} and adjusts the contrast and brightness of I^*_{f-1} such that their histograms matches. In the post-processing scheme, the method resulting in least residuals in ΔI_{f-1} is applied to I_f^*. The residual image ΔI_{f-1} also works as an estimation of the errors on the flame luminosity correction on I_{tf}.

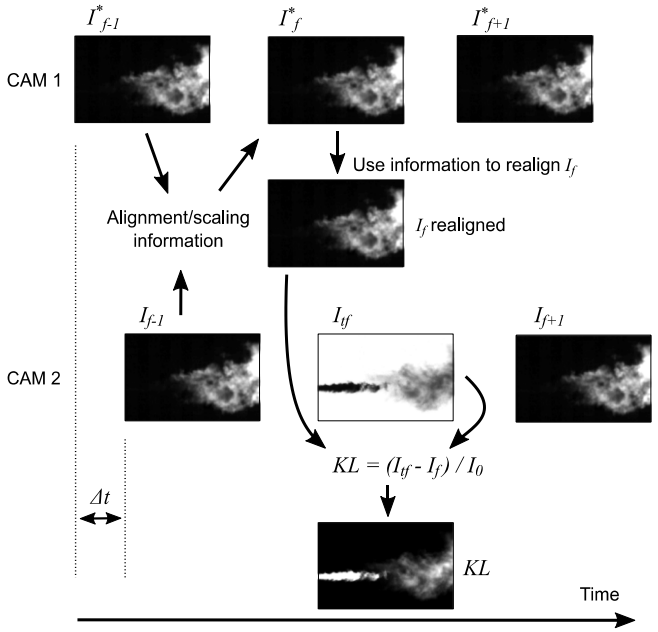

Figure 5. Post-processing procedure of images from camera 1 and 2.

Beam Steering Effects

As described earlier, the setup is designed to abate beam steering effects for angles below 50 mrad full angle by having a large enough diffuser and a Lambertian light source. These requirements have been met in the setup presented here, however, beam steering effects occurring due to intensity non-uniformities from the diffuser were also investigated. These intensity variations appear because light received by a single pixel is collected from different parts of the diffuser because of beam steering. Ideally, the spatial intensity distribution should be as uniform as possible, minimizing the intensity variation due to beam steering, but in reality the diffuser surface is imperfect, resulting in light intensity variations across the surface.

The engineered diffuser may be imagined as a plane containing a

large number of very small lenses that accept incoming light along their central axis, and output cones of light with the cone angle, in this case of 15 degrees. Due to the finite number of these lenses, the engineered diffuser essentially has a textured surface, which leads to intensity non-uniformities. This variation is also measured by the angular distribution measurement, but a more detailed analysis of the effects on the light intensity under CI-like combustion conditions is presented here.

The intensity variation during spray combustion cannot be quantified because light attenuation due to soot and beam steering effects cannot be distinguished from it. In order to quantify the intensity variation for the same beam steering that occurs during spray combustion, a model for beam steering was made. A validation of the beam steering model is done by measuring a series of premixed sootless combustion events with the light extinction setup in high speed. Since the combustion is sootless, the intensity variation due to beam steering from frame to frame can be quantified and compared to the model. Once validated, the modeled intensity variation for 50 mrad full angle beam steering is obtained and compared to other sources of uncertainty on the measured *KL* factor.

Beam Steering Model

A focused image of the diffuser surface with back-illumination is shown in the Figure 6. Each pixel on the imaging sensor receives light from an area on the diffuser surface, which is defined by the acceptance cone of the individual pixels through the collection optics. The size of the area on the diffuser subtended by the acceptance cone is determined by the aperture of the objective lens, the distance from the lens to the focal plane and the distance from the lens to the diffuser. By knowing these quantities, the un-refracted collection area can be determined. The intensity level read by the pixel is proportional to the received radiance from the collection area on the diffuser. The angular intensity distribution is in this case considered uniform within the beam steering angles that can occur (i.e. within 2.86 degrees full angle). According to Figure 3, some variation in intensity will occur due to the peaks on the edges of the angular intensity distribution (at -7.5 and 7.5 degrees). However, in the central part of the diffuser for small angle divergences, the variation is negligible.

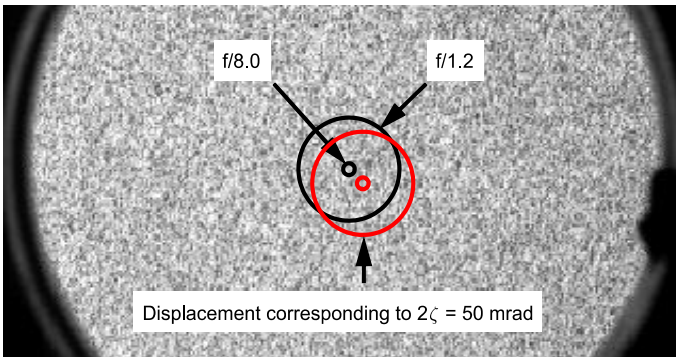

Figure 6. Intensity distribution from the diffuser surface. The collection area for f-stop f/1.2 and f/8.0 are shown. The un-refracted cases are shown as black circles, whilst the refracted cases are shown as red circles.

For the case with no beam steering, where no refractive index gradients are present within the acceptance cone, the pixel is always receiving light from the same area on the diffuser, meaning that no intensity variation is observed. For the case with beam steering, where refractive index gradients are present, the light received by the pixel is emerging from different areas of the diffuser, resulting in an intensity variation. The collection area is consequently distorted and displaced compared to the un-refracted case. The degree of distortion of the collection area is dependent on the size of the area, which is determined by the aperture of the objective lens. Since the extent of beam steering is equal for each case, a smaller collection area will be more distorted, while a larger one will be less affected. This means that the pixel receiving light from a smaller collection area, i.e. smaller aperture size, will read a higher intensity variation than that of a larger collection area. Consequently, a larger aperture is beneficial when the aim is to reduce intensity variations.

In the presented model, the distortion of the collection area is simplified by only considering displacement of the circular collection area. This simplification is equivalent to the beam steering only occurring in the focal point and having a constant refractive index gradient field, such that all light rays are refracted equally. Also the projected elliptical shape of the collection area on the diffuser when displaced has been neglected.

By using the focused image of the diffuser as input to the model, i.e. Figure 6, the average intensity level in the collection area on the diffuser was calculated. This corresponds to the pixel intensity level in the un-refracted case, i.e. no beam steering effects. For the refracted case, the collection area is displaced by a distance d, where $d = \sqrt{\Delta x^2 + \Delta y^2}$ on the x-y plane of the diffuser, as displayed in Figure 7. The beam steering angle ζ was calculated from d and the distance from the focal plane to the diffuser L by simple geometry. The spatially averaged intensity level for the refracted case is then compared to that of the un-refracted case. The resulting difference in intensity is then attributed to beam steering effects.

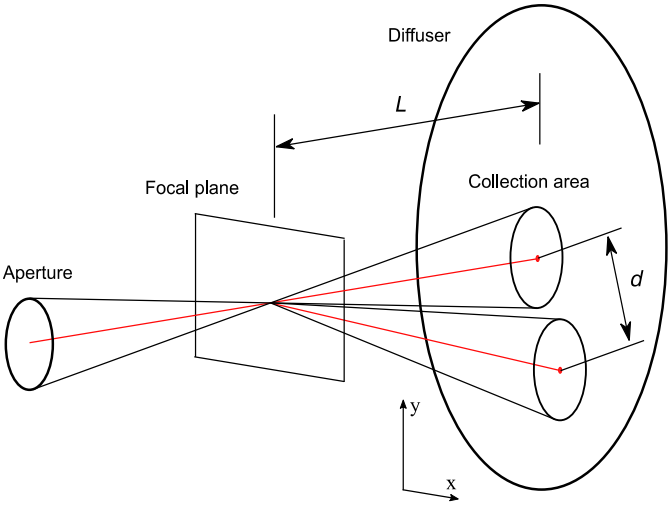

Figure 7. Schematic drawing of the beam steering model. The refracted and the un-refracted case are illustrated, with the displacement d between the collection areas.

By performing this calculation multiple times with displacements Δx and Δy following a symmetrical 2-dimensional Gaussian probability distribution function (PDF), the intensity variation due to beam steering was calculated. Musculus and Pickett [13] observed that the beam steering displacement was following an elliptical 2-dimensional Gaussian PDF, and used the geometrical mean between the major and minor diameter at 1σ to define full angle beam divergence. In the current model, a symmetrical 2D Gaussian PDF was used instead. In order to get a representable sample size for the calculation of the intensity variation, N samples of $\boldsymbol{x} = (\Delta x, \Delta y)$ following the 2D Gaussian PDF was calculated, resulting in N samples of intensity levels. The PDF $f(\boldsymbol{x})$, with its mean vector μ, its covariance matrix Σ

and a constant A is defined as

$$f(\mathbf{x}) = A\exp\left(-\frac{1}{2}(\mathbf{x}-\mu)\Sigma^{-1}(\mathbf{x}-\mu)^T\right) \quad (6)$$

$$\Sigma = \begin{pmatrix} \zeta^2 & 0 \\ 0 & \zeta^2 \end{pmatrix} \quad , \quad \mu = (\mu_x, \mu_y)^T = (0,0)^T \quad (7)$$

Experimental Setup – Sootless Combustion

The sootless combustion was achieved by running the OACIC in homogeneous charge compression ignition (HCCI) mode. Sootless combustion was used so that any changes in intensity could be attributed to beam steering effects. Although the density gradients in the HCCI combustion are assumed much smaller than in a typical diesel spray combustion event, this measurement was only used as a validation of the model. The advantage of using premixed sootless combustion compared to sootless spray combustion, was that the premixed combustion produces an uniform and consistent distribution of density gradients, making the result and validation more reliable. The model was deemed to have performed well if it could reproduce the measured intensity variations at different f-stop configurations for the same beam steering angle, since the beam steering angle is assumed similar for each HCCI combustion event.

The fuel used was a 90-10 w% iso-octane/n-heptane mixture, injected early in the combustion cycle (60 CAD BTDC). The equivalence ratio of the air-fuel mixture was 0.19. The fuel-air mixture was assumed well-mixed and all fuel fully evaporated. An acceptable repeatability of the combustion process was also verified from the cylinder pressure measurement, ensuring similar conditions during each combustion event. The HCCI combustion was imaged using DBIEI. The tests were performed with an objective lens f-stop of f/1.2, f/1.4, f/2.0, f/2.8, f/4.0, f/5.6 and f/8.0. Intensity variation due to instabilities in the light source or read noise from camera was measured and subtracted from the intensity variation measured during combustion, such that only beam steering effects were considered.

Results and Discussions

Flame Correction Tests

In order to access the errors associated with the estimated flame luminosity distribution (I_f) after applying the mean, the optical flow or the two-camera method, a sequence of flame only images was collected. This was achieved by not flashing the LED in the DBIEI setup, hence there was no back-illumination (un-illuminated). By imaging the flame luminosity with both cameras without back-illumination, the I_f obtained from the three methods were compared to the un-illuminated I_{tf} image measured by camera 2. The un-

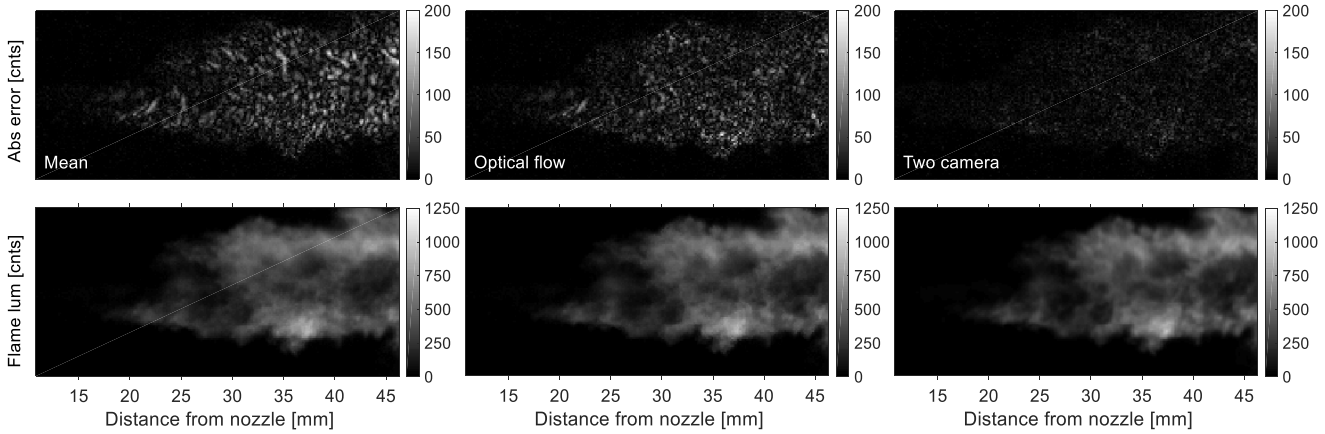

(a) Low sooting condition.

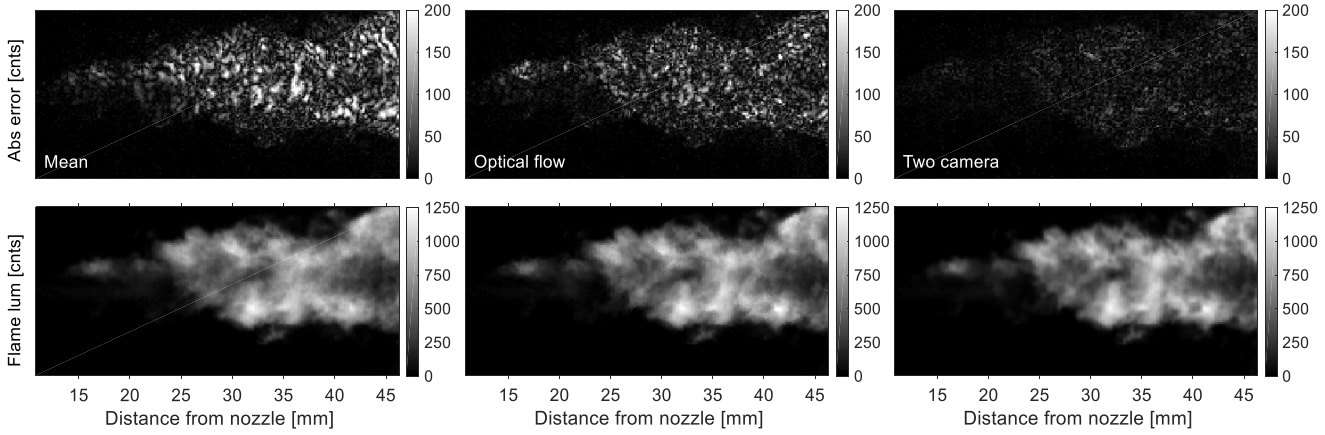

(b) High sooting condition.

Figure 8. Comparison between the absolute errors from the mean image, the optical flow and the two-camera method at 75 kfps. All values are given in counts.

illuminated image (I_{tf}) on camera 2 measures the real flame luminosity that, during DBIEI operation, is superimposed with the illuminated image when making a *KL* measurement. The mean and optical flow flame luminosity distribution were calculated from I_{f-1} and I_{f+1} on camera 2, which made it possible to compare the errors on the estimated flame luminosity from all methods. In addition to comparing the methods, this was used for optimizing the two-camera method, both the algorithm and experimental setup. The result of the test is shown in Figure 8a and Figure 8b, where the flame luminosity distributions estimated from the three methods are displayed in the bottom plots. In the top plots, the absolute error is calculated as the absolute difference between the real flame luminosity distribution and the estimated/measured one.

Figure 8 clearly shows that the errors are largest for the mean method, where the turbulent flame structures are not estimated well enough. It can also be seen that the absolute error on the flame luminosity is strongly dependent on the intensity level of the flame, resulting in higher errors on the HS condition.

Figure 10 shows plots of the pixel value (flame luminosity, in counts) along the central axis of the flame for LS and HS conditions, along with the absolute errors from the mean, the optical flow and the two-camera method along the same central axis. The characteristics of the plots shown are representative of the bulk of the estimated flame luminosities. For the LS condition, the mean and the optical flow method show similar error levels on the estimated flame luminosity, while the two-camera method is showing a lower error level. The errors are particularly larger for the mean and optical flow method where there are sudden changes in luminosity, which is explained by the relatively large time difference (13.33 µs) between I_{f-1} and I_f. The two-camera method can be seen to follow the real flame luminosity curve quite closely, but cannot capture the small spatial variations in flame luminosity and tends to spatially smooth the luminosity values. For the HS condition, the errors are larger, since the flame luminosity is generally higher. The mean method is unable to predict the intensity level of the large and sudden peaks, which are smoothened out due to the movement of the flame from the image before to after. Optical flow is predicting the peaks well, but is experiencing some difficulties at some locations, leading to relatively large errors as well. The two-camera method follows the real flame curve closely, but is smooth also for the HS condition, giving rise to errors where the real flame luminosity profile is uneven.

In order to quantify the errors from the estimation of the flame luminosity, the 90th percentile of the absolute error has been calculated for all images in an injection sequence, both for the LS and HS condition. The 90th percentile gives a measure of the level of the absolute error peaks, which defines the “worst case” of the error level. An average value of the 90th percentile during the quasi-steady part of the combustion event was used. The results are given in Figure 9. For both LS and HS condition, the optical flow method has an error level that is ~18% lower than the mean image method. The two-camera method is giving ~50% lower errors compared to optical flow method for both conditions.

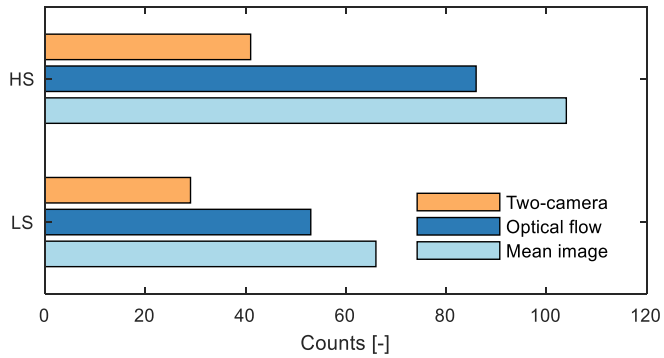

Figure 9. The average 90th percentile of the flame luminosity absolute error during the quasi-steady period.

As mentioned, the optical flow method performs better when the flame movement is small from frame to frame, i.e. optical flow can perform better if higher frame rates are used. The flame luminosity error measurement was performed with the LS condition for 100 kfps and 75 kfps, enabling optical flow to be applied to 100 kfps, 75 kfps, 50 kfps and 37.5 kfps. The 90th percentile of the absolute intensity error for the individual images were then calculated for a combustion cycle. The progression of the 90th percentile absolute error with time after SOE is shown in Figure 12, where the flame luminosity is first detected around 1500 µs after SOE. As the combustion becomes stable, at around 3000 µs, the error level of the different measurements can be compared. The error level of optical flow at 37.5 kfps is the highest, and decreases as the frame rate increases.

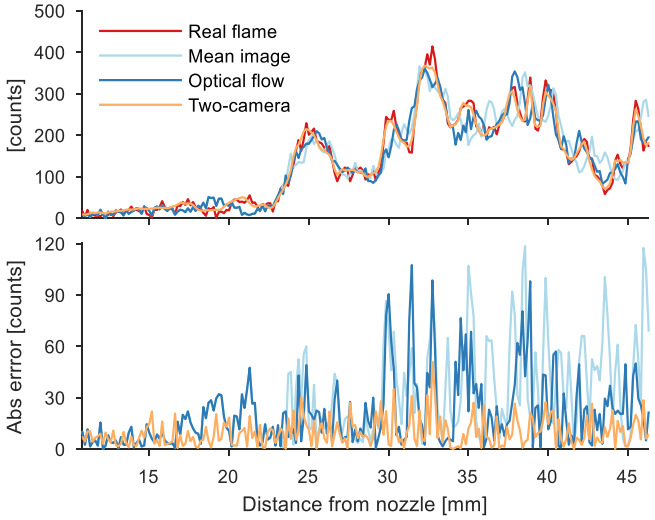

(a) Low sooting condition.

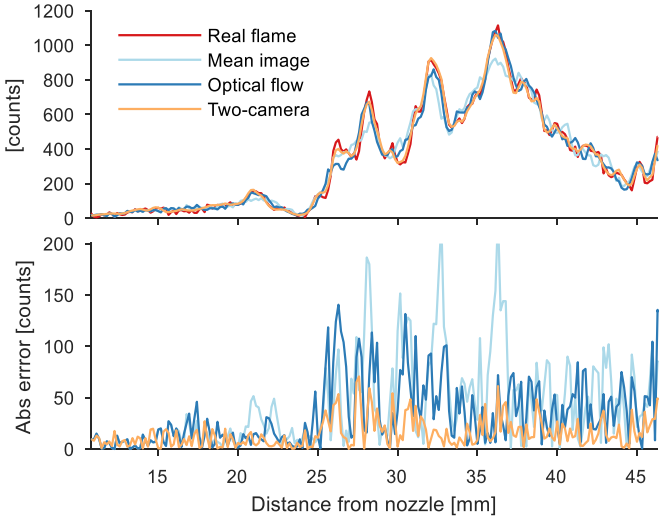

(b) High sooting condition.

Figure 10. Plots of the estimated flame luminosity and relative error along the central spray axis.

Optical flow at 100 kfps stabilizes around 41 counts, while two-camera, which was measured at 75 kfps, stabilizes around 29 counts. The dark frame read noise of the cameras has a standard deviation of approximately 5 pixel counts, and the 90th percentile of the absolute error for dark images (no flame luminosity) is 12 counts, meaning that this is the minimum value the 90th percentile can achieve in this measurement. The read noise becomes larger when a larger part of the dynamic range is used, which was not measured for the cameras used. This means that the minimum achievable absolute error might even be higher than 12 counts.

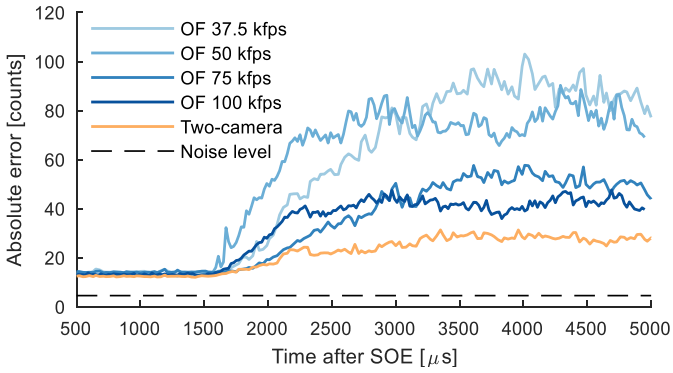

Figure 12. The progression of the 90th percentile of the absolute error on estimated flame luminosity using the optical flow method (OF) and the two-camera method for the LS condition.

Since these measurements where conducted under the same conditions, the flame luminosity level is similar for each of these tests, meaning that the relative difference between them is representable for other light extinction measurement systems or conditions where the flame luminosity to back-light intensity ratio is lower or higher.

In order for the optical flow method to approach the error level of two-camera method, a much higher frame rate is needed, which requires using a lower resolution on the measurement or using a higher specification camera. The error level of the two-camera method is also independent of frame rate, meaning that the measurement could be performed using lower specification cameras.

The biggest drawback of the two-camera method is related to the resolution. The measurement is affected by the resolution of the image since the alignment algorithm interpolates the intensity values onto neighboring pixels. The pixel grid of the moving image is not aligned with original pixel grid, meaning that the intensity values of the moved image needs to be interpolated onto the original pixel grid. In this process, some details of the flame structure are smoothed out. This effect can be minimized by increasing the resolution of the measurement as much as possible. This effect is thought to be the largest contributor to errors of the two-camera method, exceeding the errors due to the flame movement caused by the time delay between the camera exposures. The smoothing effect of the two-camera method can clearly be seen in Figure 10, where the peaks and small details along flame luminosity curve has been smoothed compared to the real flame curve.

Beam Steering Effects

Figure 11 shows the results from the beam steering model and the experimental measurements. The solid curves represents modeled relative intensity variation against full angle beam steering in milliradians. The model was calculated for 36 beam steering angles

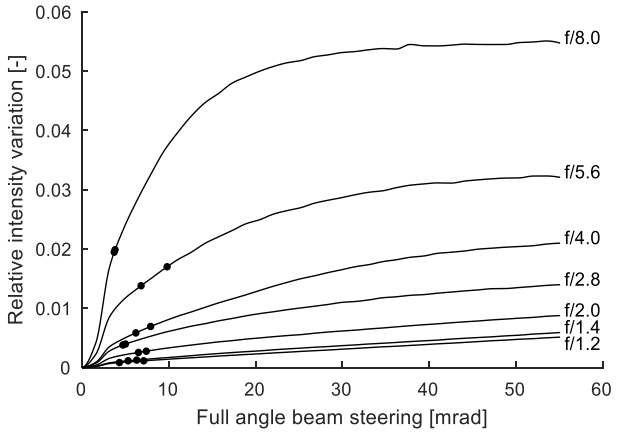

Figure 11. The solid curves represents the calculated relative intensity variation from the beam steering model. The circles along the solid curves are the measured relative intensity variations for the various f-stop configurations.

with seven f-stop configurations. Each calculation had $N = 1000$ samples per pixel, and 60 pixels on the diffuser were used, meaning that 60000 intensity levels were calculated for each case, which was found to give a converged result. The intensity levels were normalized against the mean of all samples in each pixel, and the relative intensity variation was calculated as the standard deviation of the normalized intensities for each case.

The solid curves can be observed to all start from zero intensity variation, which means that for no beam steering induced, the same collection area on the diffuser is calculated for each sample. As beam steering is induced, the intensity variation increases for all f-stops, this is due to the non-uniformity of the diffuser. The beam steering causes the collection area to move around on the diffuser according to the 2D PDF described above. The curves are all approaching a stable state as more beam steering is induced. The intensity variation for the smallest aperture (f/8.0) is observed to flatten out, reaching a maximum level of around 5.5%. For the largest aperture (f/1.2), the intensity variation reaches a linear behavior for beam steering angles larger than 10 mrad. This linear behavior is not observed for the small aperture (f/8.0) case. The reason is due to the spatial scales of the non-uniformities on the diffuser. The small aperture (f/8.0) is sensitive to small scale non-uniformities on the diffuser, because the collection area is small. Since the small scale non-uniformities are similar across the diffuser surface, the curve converges to a maximum intensity variation value. On the other hand, for the largest aperture (f/1.2), the intensity variation is most sensitive to large scale non-uniformities, since the small scale non-uniformities are averaged out by the large collection area. For the current light distribution, a slight misalignment led to a decrease in the intensity on the diffuser from one side to the other. This is observed as the linearly increasing section on the large aperture case (f/1.2), meaning that a large scale non-uniformity causes a linearly increasing intensity variation for increasing beam steering angles. For the *KL* measurements, the large scale non-uniformities for the light extinction measurements presented where considered and minimized by realignment.

The experimental results of the relative intensity variation from the HCCI combustion events are plotted on the curves as circles. This shows that the measured intensity variation corresponds to the calculated result for beam steering angles between 4 and 8 mrad, which is much lower than what is expected in a spray combustion event. The experimental results show that the model is able to calculate the same beam steering angle for several aperture sizes, meaning that the model is qualitatively validated. The relatively large

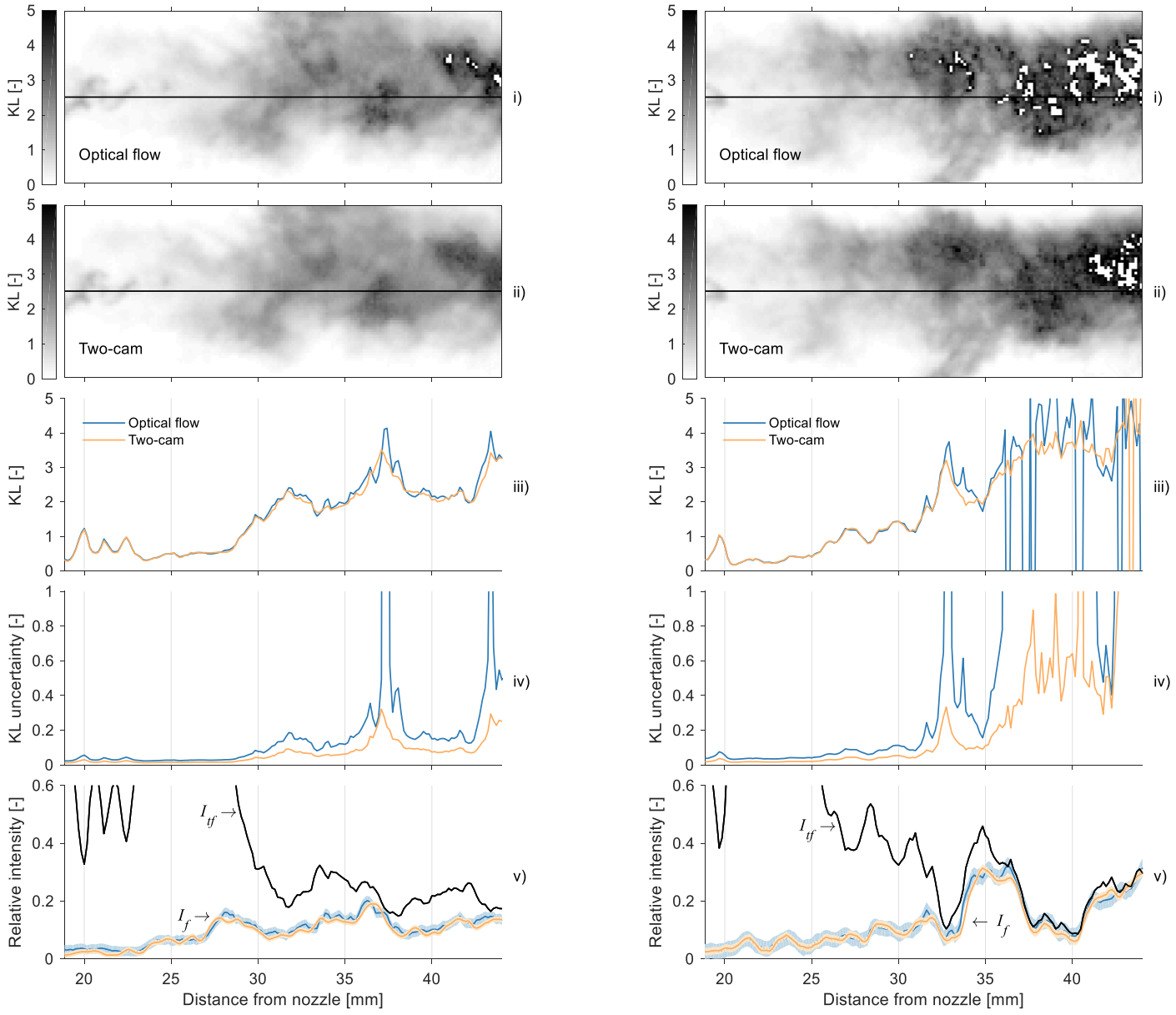

(a) Low sooting condition.

(b) High sooting condition.

Figure 13. i) *KL* plot with the optical flow method, ii) *KL* plot with the two-camera method, iii) *KL* plot through central spray axis (black line), iv) *KL* uncertainty and v) normalized I_{tf} and I_f for optical flow and two-camera method.

spread of 4 mrad on the beam steering angle could be attributed to several factors. The spread could be due to the stochastic nature of the beam steering process, or uncertainties connected to the aperture size measurement, which would greatly influence the size of the collection area for the different apertures used. Also uncertainties connected to dimensions measured in the setup can contribute to the spread observed.

For a spray combustion case, the full angle beam divergence is expected to be in the order of 50 mrad [13]. Figure 11 shows that the relative intensity variation due to 50 mrad beam steering is ~0.5% of the total intensity level. If the full dynamic range of a 12-bit camera is used, this corresponds to ~20 counts out of 4095 counts, which is below the read noise of a typical high speed camera. This confirms that the beam steering effects on the *KL* measurement due to non-uniformities of the light distribution from the engineered diffuser is negligible.

KL and Uncertainties from Flame Luminosity

Since the fuel used in this study is Diesel, a very sooty flame was expected, especially for the HS condition. A high sooting flame will emit strong broadband radiation and will greatly affect the measured I_{tf}. The absolute error on the estimated flame luminosity is observed to increase as the flame luminosity intensity increases, and the relative error is observed to be similar for low and high sooting flames. The absolute error on the estimated flame luminosity is what should be considered when investigating the impact on *KL*. Since I_f is subtracted from I_{tf} when calculating I_t, the resulting I_t is directly affected by errors on the estimated flame luminosity. If I_t is high, meaning that there is a relatively low concentration of soot in the line-of-sight, errors from the flame luminosity has a low impact on

the calculated *KL*. On the contrary, when I_t is low, meaning that there is a high concentration of soot in the line-of-sight, the errors from the flame luminosity will have a large impact on *KL*. In sum, high sooting regions suffer from both high sensitivity on I_t and larger errors on the estimated flame luminosity I_f.

Samples of *KL* distributions for the LS and HS conditions are presented in Figure 13a and Figure 13b, respectively. *KL* is shown when the optical flow and the two-camera method have been applied, for both conditions, i.e. plots i) and ii). The *KL* distributions are shown for the downstream part of the spray, i.e. the injector nozzle is located on the left hand side of the plot. The end of the liquid core can be observed up to about 25 mm downstream of the nozzle for LS and 20 mm for HS. Any attenuation downstream from these points is expected to be attenuation of light due to the presence of soot. As the spray moves further downstream, *KL* increases for both conditions.

White spots in dark regions of the *KL* plot indicates where I_f is estimated to be higher than I_{tf}, which in turn results in I_t becoming negative and *KL* becoming a complex number. This occurs in regions where the real I_t/I_0 is low (~2-3%). The unphysical result of a negative I_t is mainly due to errors from the flame estimation. The three plots, iii), iv) and v), displayed below the *KL* distribution show the plot of *KL* along the spray central axis (black line on the *KL* images), the uncertainty of *KL* along the central axis and the normalized I_{tf} and I_f along the central axis. The uncertainty of *KL* is calculated as a "worst case scenario" based on values from Figure 9. Based on the 90th percentile absolute error on the flame luminosity, the real I_f will be within $I_f \pm \varepsilon$, where ε is the 90th percentile absolute error on the estimated flame luminosity. The corresponding uncertainty on *KL* can then be calculated as:

$$\varepsilon_{KL} = \frac{1}{2}\left(-\ln\left(\frac{I_{tf} - I_f - \varepsilon}{I_0} \right) + \ln\left(\frac{I_{tf} - I_f + \varepsilon}{I_0} \right) \right) \quad (8)$$

The *KL* plot along the spray central axis for LS shows that optical flow and two-camera method yields similar results, except at the peaks, where optical flow method is deviating a lot from the two-camera method. However, since the real *KL* is unknown, it is not possible to determine which one is incorrect by the largest amount. By looking at the *KL* uncertainty plot, which is calculated based on Equation 8, the two-camera method shows a relatively low uncertainty compared to the optical flow method, in particular around the peaks.

For the HS condition, the same behavior can be spotted at the first *KL* peak, where the optical method is yielding a relatively large *KL* value compared to two-camera method. The *KL* values calculated with the optical method further downstream are showing multiple regions with negative values of I_t, which suggests that the flame estimation is affecting *KL*. This is confirmed when looking at the *KL* uncertainty plot, where the uncertainty for optical flow is large and unbounded. For two-camera method, the uncertainty on *KL* is also relatively large in this region, but bounded. This region is the upper soot attenuation limit for the measurement system ($KL \approx 3.8$). The upper limit of the measurement system is mainly limited by the imaging sensors sensitivity. The *KL* uncertainty for two-camera stays relatively stable over the high sooting region, with a value of around 0.5.

In order to measure high values of *KL*, a very accurate estimation of the flame luminosity is needed. The two-camera method is showing a great improvement to the measurement technique for these regions. For lower values of *KL*, two-camera still outperforms the optical flow method, where the uncertainty is observed to be half compared to the optical flow method. The uncertainty on *KL* when using optical flow for *KL* values above 2.7 in this measurement cannot be trusted, and should be disregarded.

Conclusions

In the present study, sources of error on *KL*, such as the flame luminosity effect and the beam steering effect, has been studied in detail. A new method for correcting for the flame luminosity influence on *KL* has been presented, which involves measuring the flame luminosity with a separate camera, i.e. the two-camera method. Also, a model for calculating intensity variations in the transmitted intensity caused by changes in refractive index (beam steering effects), has been presented.

A comparison between the mean image, the optical flow and two-camera method was made. The mean image method yields the highest absolute errors to the flame luminosity correction, while the optical flow method shows a decrease of ~18% compared to the mean image method. The two-camera method yields the lowest absolute error and is ~50% lower than the optical flow method. This is independent of the flame luminosity intensity level.

The larger errors from the optical flow method are attributed to the relatively large time step between the flame luminosity frames. These errors were shown to decrease as the frame rate of the measurement increased, decreasing the time step. Measuring the absolute errors from the optical flow method at 100 kfps still gave a higher error level compared to the two-camera method, which was ~30% lower.

The mean image and the optical flow method are not able to estimate the real flame luminosity intensity in regions of the flame where the flame luminosity has sudden changes, consequently failing to estimate the flame luminosity peaks. The two-camera method follows the real flame luminosity distribution closely, but is not able to capture small variations in the flame structure. The bulk of the errors associated with the two-camera method was found to be due to a smoothing effect, caused by the alignment algorithm. A higher resolution of the flame image reduces these errors. The alignment of the two cameras also showed to be very important in order to minimize the error level.

The impact of flame luminosity correction errors on *KL* was investigated. The uncertainty on the measured *KL* was found to be highest for regions in the flame where the highest concentration of soot was present. In these regions, the flame luminosity intensity was generally higher compared to regions with lower *KL* values, which gave rise to higher absolute errors from the flame luminosity correction. Combined with the fact that the transmitted light intensity is lower for the same regions, these regions are in particular prone to uncertainties. The uncertainty on *KL* by using the optical flow method was approximately 100% higher than when using two-camera method. For *KL* values above 2.7, the optical flow method did not give a bounded uncertainty, while the two-camera method had acceptable uncertainties up to 3.8.

The beam steering model was qualitatively validated by experiments, and shows the importance of having a large collection angle that results in a large collection area on the diffuser surface. The large collection area reduces intensity variations caused by small scale non-uniformities in the light output from the diffuser. The model also shows the importance of minimizing large scale non-uniformities in

the light source output, which is observed to cause intensity variations to the measurement. The model also verified that the intensity variations caused by beam steering for the current setup could be neglected under typical CI spray combustion conditions.

References

1. Hottel, H.C. and Broughton, F.P., "Determination of True Temperature and Total Radiation from Luminous Gas Flames Use of Special Two-Color Optical Pyrometer," *Ind. Eng. Chem. Anal. Ed.* 4(2):166–175, 1932.

2. Payri, F., Pastor, J. V, García, J.M., and Pastor, J.M., "Contribution to the application of two-colour imaging to diesel combustion," *Meas. Sci. Technol.* 18(8):2579–2598, 2007, doi:10.1088/0957-0233/18/8/034.

3. Kosaka, H., Aizawa, T., and Kamimoto, T., "Two-dimensional imaging of ignition and soot formation processes in a diesel flame," *Int. J. Engine Res.* 6(1):21–42, 2005, doi:10.1243/146808705X7347.

4. Sjöholm, J., Wellander, R., Bladh, H., Richter, M., Bengtsson, P.-E., Alden, M., Aronsson, U., Chartier, C., Andersson, O., and Johansson, B., "Challenges for In-Cylinder High-Speed Two-Dimensional Laser-Induced Incandescence Measurements of Soot," *SAE Int. J. Engines* 4(1):1607–1622, 2011, doi:10.4271/2011-01-1280.

5. Musculus, M.P., Dec, J.E., and Tree, D.R., "Effects of Fuel Parameters and Diffusion Flame Lift-Off on Soot Formation in a Heavy-Duty DI Diesel Engine In-Cylinder Diesel Particulates and NOx Control," *SAE Trans.* 111(3):1467–1489, 2002, doi:10.4271/2002-01-0889.

6. Zhao, H. and Ladommatos, N., "Optical diagnostics for soot and temperature measurement in diesel engines," *Prog. Energy Combust. Sci.* 24(3):221–255, 1998.

7. Manin, J., Pickett, L.M., and Skeen, S.A., "Two-Color Diffused Back-Illumination Imaging as a Diagnostic for Time-Resolved Soot Measurements in Reacting Sprays," *SAE Int. J. Engines* 6(4):2013-01-2548, 2013, doi:10.4271/2013-01-2548.

8. Greenberg, P.S. and Ku, J.C., "Soot volume fraction imaging," *Appl. Opt.* 36(22):5514, 1997, doi:10.1364/AO.36.005514.

9. Xu, Y. and Lee, C.F., "Forward-illumination light-extinction technique for soot measurement," *Appl. Opt.* 45(9):2046, 2006, doi:10.1364/AO.45.002046.

10. Thomson, K.A., Johnson, M.R., Snelling, D.R., and Smallwood, G.J., "Diffuse-light Two-dimentional Line-of-sight Attenuation for Soot Concentration Measurements," *Appl. Opt.* 47(5):2–11, 2008.

11. Ghandhi, J.B. and Heim, D.M., "An optimized optical system for backlit imaging," *Rev. Sci. Instrum.* 80(5):80–83, 2009, doi:10.1063/1.3128728.

12. Westlye, F.R., Penney, K., Ivarsson, A., Pickett, L.M., Manin, J., and Skeen, S.A., "Diffuse back-illumination setup for high temporally resolved extinction imaging," *Appl. Opt.* 56(17):5028, 2017, doi:10.1364/AO.56.005028.

13. Musculus, M.P.B. and Pickett, L.M., "Diagnostic considerations for optical laser-extinction measurements of soot in high-pressure transient combustion environments," *Combust. Flame* 141(4):371–391, 2005.

14. Westlye, F.R., "Experimental Study of Liquid Fuel Spray Combustion," Technical University of Denmark, 2016.

15. Pastor, J. V., Garcia-Oliver, J.M., Novella, R., and Xuan, T., "Soot Quantification of Single-Hole Diesel Sprays by Means of Extinction Imaging," *SAE Int. J. Engines* 8(5):2015-24–2417, 2015, doi:10.4271/2015-24-2417.

16. Pastor, J.V., Garcia-Oliver, J.M., Garcia, A., and Pinotti, M., "Soot Characterization of Diesel/Gasoline Blends Injected through a Single Injection System in CI engines," *SAE Tech. Pap.* (2017-24-0048), 2017, doi:10.4271/2017-24-0048.

17. Skeen, S.A. and Yasutomi, K., "Measuring the soot onset temperature in high-pressure n-dodecane spray pyrolysis," *Combust. Flame* 188:483–487, 2018, doi:10.1016/j.combustflame.2017.09.030.

18. Pandurangi, S.S., Bolla, M., Wright, Y.M., Boulouchos, K., Skeen, S.A., Manin, J., and Pickett, L.M., "Onset and progression of soot in high-pressure n-dodecane sprays under diesel engine conditions," *Int. J. Engine Res.* 18(5–6):436–452, 2017, doi:10.1177/1468087416661041.

19. ECN Website. Accessed on 23.04.2018. URL: http://www.sandia.gov/ecn/index.php.

20. Skeen, S.A., Manin, J., Dalen, K., and Pickett, L.M., "Extinction-based Imaging of Soot Processes over a Range of Diesel Operating Conditions," *8th US Natl. Combust. Meet.* 1–13, 2013.

21. Willert, C., Stasicki, B., Klinner, J., and Moessner, S., "Pulsed operation of high-power light emitting diodes for imaging flow velocimetry," *Meas. Sci. Technol.* 21(7):075402, 2010, doi:10.1088/0957-0233/21/7/075402.

22. Sun, D., "Secrets of Optical Flow Estimation and Their Principles • Optical flow : motion of image pixels," *Proc. IEEE Comput. Soc. Conf. Comput. Vis. Pattern Recog.* 2432–2439, 2010.

Contact Information

Karl Oskar Pires Bjørgen
karl.o.bjorgen@ntnu.no
Phone: +47 90861780

Acknowledgements

The experiments were conducted in the Motorlab at the Norwegian University of Science and Technology in Trondheim, Norway. The

laboratory is supported by the research center Bio4fuels, which is part of Centres for Environment-friendly Energy Research (FME) funded by the Norwegian Research Council.

Abbreviations

BTDC	Before top dead center
CAD	Crank angle degree
CCD	Charge-coupled device
CI	Compression ignition
DBIEI	Diffuse back-illuminated extinction imaging
ECN	Engine Combustion Network
FME	Forskningssentre for miljøvennlig energi
FWHM	Full width at half maximum
HCCI	Homogeneous charge compression ignition
HS	High sooting
LE	Light extinction
LED	Light emitting diode
LS	Low sooting
ND	Neutral density
NL	Natural luminosity
NTNU	Norges Teknisk-Naturvitenskaplige Universitet
OACIC	Optical accessible compression-ignited chamber
OD	Optical density
PDF	Probability density function
PLII	Planar laser-induced incandescence
SOE	Start of energizing
TDC	Top dead center